IAC–18–C1.9.12

ADAPTED SYZYGY FUNCTIONS FOR THE PRELIMINARY DESIGN OF MULTIPLE GRAVITY ASSISTED TRAJECTORIES

Davide Menzio
Politecnico di Milano, Italy
davide.menzio@polimi.it

Camilla Colombo
Politecnico di Milano, Italy
camilla.colombo@polimi.it

Abstract. In the design of Multiple Gravity Assisted (MGA) trajectories, the most critical and time-consuming phase is the definition of the sequence of planets at which to perform the flybys. A general approach tackles the MGA problem using a branch and bound technique to resolve the combinatorial problem arising by the possible sequences of planets to be flown in order to reach the destination in reasonable amount of time. It is clear how, depending on the associated launch window and the total time of flight, not a unique optimal configuration exists. Possible solutions are searched selecting each planet at a time, resolving the associated Lambert problem for a specific time of flight and choosing the minimum delta-v solution. Such an approach is extremely expensive from a computational point of view: depending on the orbital distance to be reached and the associated number of planets that could be flown, the process requires at each stage the evaluations of the remaining possibilities in cascade and for different encounter epochs. The goal of this paper is to provide a quick estimate of the possible planet configurations for the preliminary design of suboptimal MGA trajectories. For such purpose, the syzygy function, commonly used in astronomy for the identification of planet alignment, is mimicked and adapted to satisfy the needs of trajectory design. Different strategies to exploit this approach are presented. At a first stage, a simple modification of the classical syzygy function is considered: the alignment condition is maintained but with a time shift, ensuring that, between one planet and the following one, the time of flight between two planets is exactly a Hohmann semi-period. The limitation of this approach, which always enforces a Hohmann transfers between one planet and the following, is resolved by the use of a shape-based approach for the trajectory model, which modifies the syzygy line condition into a conic section one. Shaping the trajectory on the eccentricity allows to select the time of interception by resolving the time equation. The use of additional constraints on the relative velocity at flyby of the planet belonging to the defined sequence is considered to further limit the number of preliminary solutions. The proposed approaches is tested on an Venus-Earth-Jupiter trajectory, in the flavour of the Cassinis mission.

1. Introduction

A method to achieve a fast progress in a specific discipline is to steal a technique from others and find a way to apply to the specific problem we are considering. Several examples comes from the field of optimization, which mimicked a controlled evolution process, to develop interesting tools such as genetic algorithm (GA), differential programming and particle swarm optimisation, to quote the most famous.
The idea behind the paper is similar, even if less intrepid. Looking for a method to compute the synodic period for more than two planets, we came across to a method used in astronomy to identify combination of visible planets. The beauty of the method consists in describing the problem through a simple function and study where it tends to zero.
Considering the area of mission analysis and in particular the design of multiple gravity assisted trajectories, it would be extremely useful to reduce the problem of the flyby to a simple zero function.

A general approach infact tackle the problem of the flyby in a combinatorial manner whose exploration of the full solutions results unpractical not to say impossible, a fortiori, if it is taken into account that identification of a sequence must be anyway refined in higher dynamics through optimisations. Over the years, several methods were proposed to simplify the design of the flyby in the circular restricted three body problem dynamics, with the keplerian map [1],

the Tisserand-Poincaré map [2] and the flyby [3] and kick map [4] for low energy flyby. Nevertheless, the above methods offer a solution which depends on the parameter state vector (e.g. initial epoch, position, velocity) and therefore require to be repeated for each initial condition to give a representation of the solution in "global" map.

The objective of this paper is to show that it is possible to construct a simple function to analyse a broad set of initial/final conditions and quickly identify planetary configuration for feasible trajectory undergoing a single or multiple flyby and the paper is organised as follow. In the first section, the usual syzygy function used in astronomy is presented and applied to two scenarios (three and four planets). In the third section, a first attempt to pass from the line of view to a special conic section is achieved through the Hohmann-syzygy. In the end, an attempt to pass from the straight line to a conic condition is analysed.

2. The syzygy

The alignment of three or more planets is usually called a syzygy in astronomy, from *σύζυγος* (*súzugos*, "conjunction") in Ancient Greek.
Such condition occurs when the planets, 1. 2. and 3. , form a straight-line while revolving about the Sun.

$$\begin{aligned} 1.: & \begin{cases} x_1 = r_1 \cos\left(n_1 t + \varphi_1\left(t, t_0\right)\right) \\ y_1 = r_1 \sin\left(n_1 t + \varphi_1\left(t, t_0\right)\right) \end{cases} \\ 2.: & \begin{cases} x_2 = r_2 \cos\left(n_2 t + \varphi_2\left(t, t_0\right)\right) \\ y_2 = r_2 \sin\left(n_2 t + \varphi_2\left(t, t_0\right)\right) \end{cases} \\ 3.: & \begin{cases} x_3 = r_3 \cos\left(n_3 t + \varphi_3\left(t, t_0\right)\right) \\ y_3 = r_3 \sin\left(n_3 t + \varphi_3\left(t, t_0\right)\right) \end{cases} \end{aligned} \tag{1}$$

Given their positions, x and y, as function of the orbital radius, r, the angular velocity, n and the phasing angle φ measured at time t from the alignment time t_0, see (1), then the line-configuration can be expressed via the equation of the line passing from three points, see (2).

$$\frac{x_1 - x_2}{y_1 - y_2} = \frac{x_3 - x_2}{y_3 - y_2} \tag{2}$$

Rearranging (2) by making the denominator vanishing and by exploiting the trigonometric identity, the syzygy function can be written as a summation of sine of the angular difference of the planets, see (3):

$$\begin{aligned} f_{123} = & \frac{\sin\left[\left(n_3 - n_2\right) t + \varphi_{32}\right]}{r_1} + \ldots \\ & \frac{\sin\left[\left(n_1 - n_3\right) t + \varphi_{13}\right]}{r_2} + \ldots \quad \to 0 \\ & \frac{\sin\left[\left(n_2 - n_1\right) t + \varphi_{21}\right]}{r_3} \end{aligned} \tag{3}$$

and identifies a planetary alignment when it tends to zero, as you can see from Fig. 1 and Fig. 2.

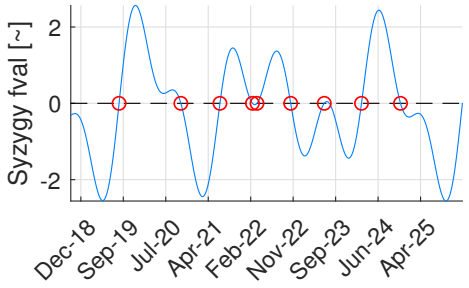

Figure 1: Evolution of in time of the syzygy function for Earth, Venus and Mars alignment

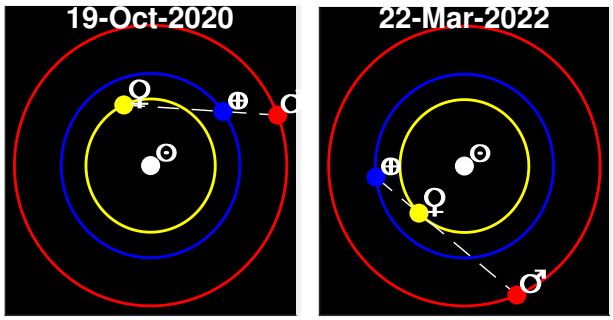

Figure 2: Two alignments of Earth, Venus and Mars identified at the zeros of the syzygy function, see Fig. 1

The alignment of more than three planets are extremely rare in occurrence. Nevertheless, it is possible to build a syzygy function by using the sum of square principle which measure the non-linearity of two three-planet Syzygies, see (4):

$$F\left(t\right) = f_{123}\left(t\right)^2 + f_{124}\left(t\right)^2 \to 0 \tag{4}$$

By representing the evolution of the syzygy with the time, Fig. 3 shows that two possible solutions can be considered: those identified by a "perfect" (dependent on the solver tolerance) alignment identified by the $\star$ marker, and minima that are close to the zero but that doesn't nullify the syzygy.

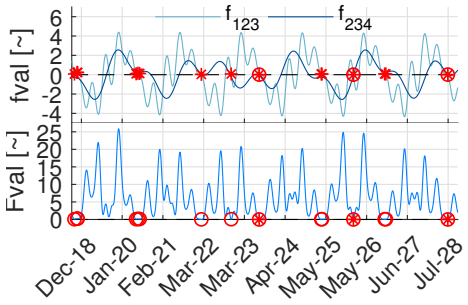

Figure 3: Evolution of in time of the syzygy function for Mercury, Venus, Earth and Mars alignment. The $\star$ markers identifies where $F(t)$ has effectively converged to zero, while the o one shows local minima, close to zero but not approaching its value

Despite only $\star$ solutions should be considered as alignments, for the purpose of sighting, o ones might represent already good enough one, see Fig. 4. Attentions must be paid in selecting a value close to zero, due to the composition with the sum square (0.002 was choosen for this particular case).

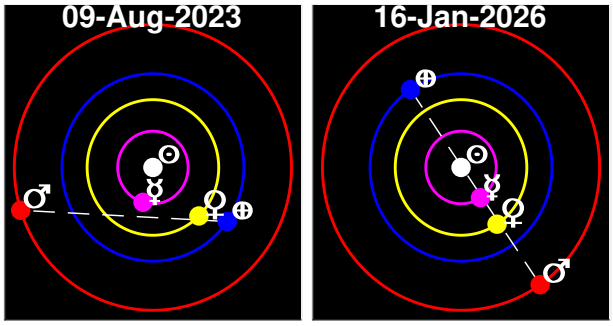

Figure 4: Two alignments of Mercury, Venus earth and Mars identified by the $\star$ markers at the zeros of the syzygy function, see Fig. 3

Of course, the syzygy doesnt account for orbital eccentricities, or for inclinations of the orbits from the ecliptic, but it does give a general idea of the patterns of alignment that would be expected for planets with roughly circular and coplanar orbits.

3. From astronomy to mission design

The beauty of the syzygy function consists in the ability to identify specific configuration of planets taking into accounts their dynamics. Therefore, an application in mission analysis could be interesting in order to identify in a quick way feasible trajectories for the exploration of the planets.

3.1 The time augmentation

Since warp drive is still unpractical for actual space-ship, at least for now, the syzygy function has to consider the time of flight to reach the planet. Preserving the line-condition imposes to follow Hohmann trajectory from one planet to the next.

Differently from the sighting problem, it must be noticed that the dynamics requires the Sun to be in line with the flown bodies. Such requirement allows to write the zero function as a simplified version of the four planets syzygy (5):

$$F(t) = \sum_{j=1}^{n_{Pl}-1} \left(r_j r_{j+1} \sin\left(n_{j+1} tof_j + \varphi_{j,j+1}(t_j)\right)\right)^2 \tag{5}$$

3.2 Limitation

Such expression presents some drawbacks. First of all, it doesn't have any information about the disposition of the bodies under study, which must be analysed in order to ensure that it respects the sequence imposed by the time of flights. In other words, it might occur that the three planets are actually aligned, as expect from the Hohmann-syzygy approaching the zero, see Fig.5 but planets are not in an Hohmann-configuration, which requires to ride on an unfeasible high-eccentricity and high-inclination orbit, see Fig.6.

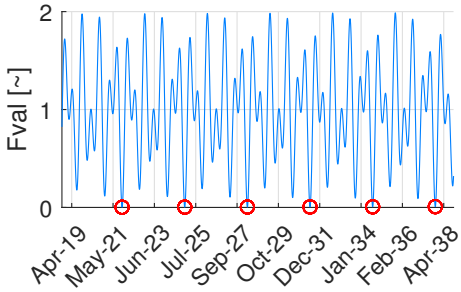

Figure 5: Evolution of in time of the Hohmann-syzygy function for Earth, Venus, Mars transfer

Secondly, the restriction imposed by the line-condition limits the possible trajectory to a sequence of Hohmann transfers. With arrival and departure velocities at the planet not only parallel but tangential to the orbit, the flyby flyby gives no contribution, see (6):

$$\Delta v_{fby} = v_\infty \sin 2\delta \tag{6}$$

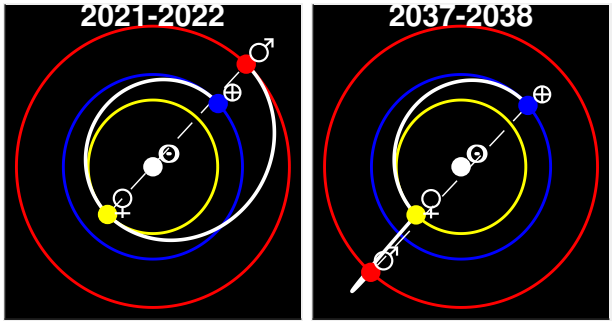

Figure 6: The solutions identified from the Hohmann-syzygy function: on the left the correct disposition of the planets allows to perform two Hohmann to reach Mars, on the right having Venus and Mars from the same side results the bouncy trajectory

Therefore the difference in term of heliocentric velocity must be provided by the propulsion system and in a general sense the trajectory is not optimal. Nevertheless, it has to be considered that if the syzygy doesn't converge to zero exactly to zero, then the flyby does give a contribution, however small, and that even when it does low-energy flyby could take place and these effects might modify the Hohmann transfer in a significant way. It's clear that Hohmann syzygy more than a solution to the trajectory design represents an exercise to apply a resolution method for a mission design problem keeping a similar formulation of the astrodynamical one, which obviously has to be modified.

4. From line to conic condition

It's clear that the line-condition must be abandoned in spite of a conic-one. Such improvement of the policy complicates significantly the search of feasible transfer. To do that, a staged approached is applied. The main idea behind this section is to shape the trajectory and use the new syzygy function to identify where time of flight meet the time of interception, similarly to what done previously.

At first, an attempt to determine the configuration of the planets so that they describe a unique orbit is performed. Secondly, the orbit is treated as two distinct trajectories that merge at the flyby.

4.1 One ellipse and three coplanar positions

Considering a single flyby problem, the unique trajectory represents the degenerate solution such that the flyby gives no contribution. Differently from the consecutive Hohmann transfers orbit, this time, no delta-v must be applied to continue to the following planet. Selected three planets and given the evolution of their angular position with the respect of the time, see (7):

$$\begin{array}{lll} 1.: & r_1 & L_1 = n_1 t_1 + \varphi_1(t_0) \\ 2.: & r_2 & L_2 = n_2 t_2 + \varphi_2(t_0) \\ 3.: & r_3 & L_1 = n_3 t_3 + \varphi_3(t_0) \end{array} \tag{7}$$

where L represents the true anomaly of the planet and at the same time the longitude of the transfer orbit. It is possible to compute the associated semi-latus rectum, p, eccentricity e and periapsis argument ω, from the linearised-orbit equation, see (8):

$$\frac{p}{r_i} - f\cos L_i - g\sin L_i = 1 \tag{8}$$

where f and g constitute the components of the eccentricity vector. By applying the Crame's rule and classical trigonometry identities [5], it can be shown that the equinoctial elements can be derived as function of the true longitudes, L_1, L_2 and L_3, and therefore of departure, encounter and arrival time t_1, t_2 and t_3 respectively, see (9):

$$\begin{cases} p = \frac{r_1 r_2 r_3(\sin L_2 - L_1 + \sin L_1 - L_3 + \sin L_3 - L_2)}{r_1 r_2 \sin L_2 - L_1 + r_1 r_3 \sin L_1 - L_3 + r_2 r_3 \sin L_3 - L_2} \\ f = \frac{r_1(r_2 - r_3)\sin L_1 + r_2(r_3 - r_1)\sin L_2 + r_3(r_1 - r_2)\sin L_3}{r_1 r_2 \sin L_2 - L_1 + r_1 r_3 \sin L_1 - L_3 + r_2 r_3 \sin L_3 - L_2} \\ g = \frac{r_1(r_3 - r_2)\cos L_1 + r_2(r_1 - r_3)\cos L_2 + r_3(r_2 - r_1)\cos L_3}{r_1 r_2 \sin L_2 - L_1 + r_1 r_3 \sin L_1 - L_3 + r_2 r_3 \sin L_3 - L_2} \end{cases} \tag{9}$$

Since the space triangles are defined by the differences in true longitude, , and the semi-major axis, a, the time of flights can be directly derived from the Kepler's equation, in fact see (10):

$$tof_{21} = \sqrt{\frac{a^3}{\mu}}\left(\alpha - \beta - \sin\alpha + \sin\beta\right) \tag{10}$$

where α and β depend uniquely on L_2 and L_1 [6]. Similarly for tof_{32}.

Feasible transfer condition (FTC) for the short transfer arc can be identified where the time of flight satisfy the time of encounter with the planet, see (11):

$$\begin{array}{lll} FTC_{12} = & \cos\left(n_2 tof_{21} + \varphi_{21}(t_1)\right) + \\ & -\cos\left(L_2(t_2) - L_1(t_1)\right) \\ s.t. & \sin\left(n_2 tof_{21} + \varphi_{21}(t_1)\right) > 0 \end{array} \tag{11}$$

Long transfer solutionscan be obtained substituting the tof_{21} with its complementary, with the respect of the period and changing the sign to the disequality. The syzygy function for the unique orbit case identifies unique trajectory where both the FTC tend to zero, which can be written as, see (12):

$$F(t) = FTC_{12}^2 + FTC_{23}^2 \to 0 \tag{12}$$

Considering a potential trajectory from Venus to Jupiter, passing from Earth, in the flavour of Cassini's trajectory to Saturn ($3^{\text{rd}} - 4^{\text{th}}$ legs), a possible syzygy-solution for the degenerate flyby orbit can be obtain in 2023, see Fig.7.

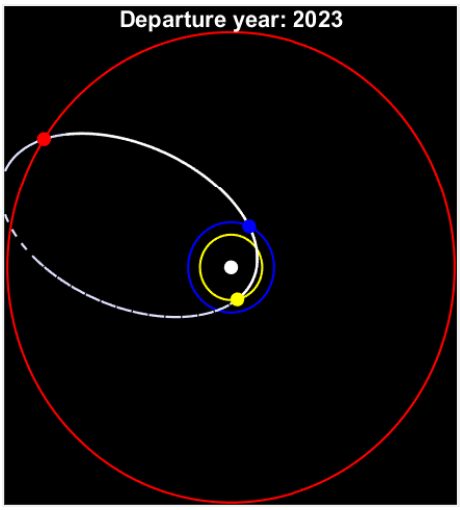

Figure 7: The solution for the unique ellipse syzygy applied to a degenerate Venus-Earth-Jupiter trajectory.

4.2 Two ellipse and a flyby

Considering the effect of the flyby, requires to evaluate two individual orbits whose difference in orbital elemenets should be addressed to flyby effect. If previously the number of variables where six (three for the orbital elements, two for the times of flight and one for the initial date, which represented the real design parameter) now it grows to ten (three more for the post-flyby trajectory and one for the peri-apsis passage, r_p, or turning angle, δ, at the encounter).

As it is the problem admits infinite solutions, since the number of variables is greater than the number of unknowns. Therefore, some additional constraints should be taken into account to balance the two and, in view of providing a solution as close as possible to the optimal one, whether it exists, only tangential arcs are considered at the terminal points (departure and arrival).

Differently from the single orbit case, in which the orbital elements were obtained directly as a function of the time, here, such considerations cannot hold and an orbital element must be chosen parametric to efficiently shape the orbits. The eccentricity represents the best option. Considering the tangential arc condition , the eccentricity and the departure/arrival date solely, determine in a clear way the two trajectories. With the semi-major axis depending on the eccentricity only and the argument of the periapsis on the departure date, see (13), the aperture of space triangle, identified by the difference of the true longitude, can be obtained replacing the semi-major axis in the orbit equation and resolving for the true anomaly difference, see (14).

$$a_1(e1) = \frac{r_1}{1-e_1} \qquad \omega_1(t_1) = L_1(t_1) \tag{13}$$

$$\cos(\Delta L_{21}(e_1)) = \frac{1}{e_1}\left(\frac{r_1}{r_2}(1+e_1) - 1\right) \tag{14}$$

It can be noticed that the condition of existence of the cosine in (14) imposes that the right term cannot be greater/smaller than $+1/-1$ from which the minimum and maximum eccentricity values are derived, see (15).

$$\frac{1}{e_1}\left(\frac{r_1}{r_2}(1+e_1) - 1\right) = \begin{cases} 1 \rightarrow e_m = \frac{r_2 - r_1}{r_2 + r_1} \\ -1 \rightarrow e_M = 1 \end{cases} \tag{15}$$

The FTC (11) correlates the shaping parameter with the epoch of departure, see Fig.8 which represents the solution for the first leg of Venus-Earth-Jupiter trajectory:

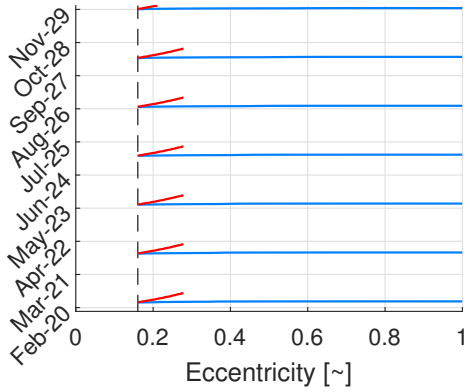

Figure 8: The solution for the feasible short (light blue, solid) and long (red solid) transfer condition for the Venus-Earth leg, limited to an Hohman period time of flight [7].

and provide the solution for the feasible trajectory, see (16), in term of the semi-major axis, argument of the periapsis from (13) and arrival epoch from time of flight from (10).

$$FTC_{21}(e_1, t_1) = 0 \rightarrow [e_1^*, t_1^*, t_2^*, a_1^*, w_1^*] \tag{16}$$

For the Venus-Earth leg, the constrained value of the time of flights and the associated semi-major axis can be represented as eccentricity related parameters, see Fig.9,

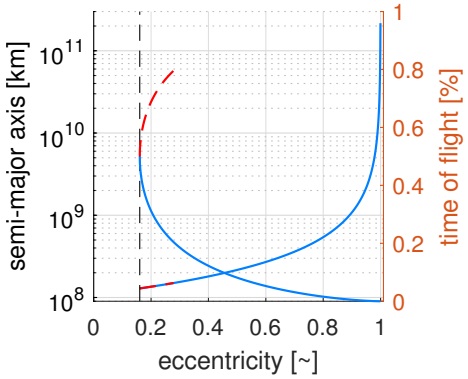

Figure 9: The dependency of the semi-major axis and the associated time of flight on the eccentricity for the Venus-Earth leg tangential at the departure. In the light blue, solid line the solution for the short transfers while in red dashed line the long one

Paying attention to the sign of the sine of the aperture that for negative values imposes to replace the time of flight with its complementary value with the respect of the period (long transfer).

And finally the associated pork-chop expressed in dates of departure from Venus and pre-encounter with Earth, t_1^* and t_2^*, obtained for the tangential departure hypothesis, can be represented in Fig.10:

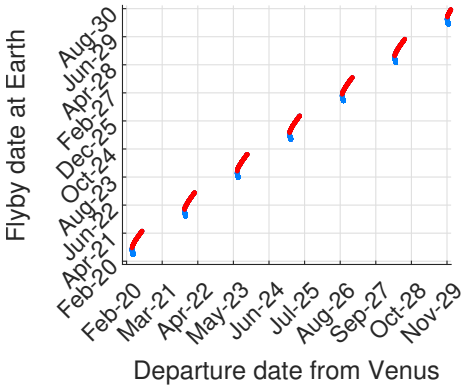

Figure 10: The pork-chop plot representation of the short transfer solutions (light blue, solid) and long arc ones (red solid) for the Venus-Earth leg

Similar reasoning can be done considering a tangential arrival at Jupiter and, again, parametrising the Earth-Jupiter leg on the eccentricity, see (17) and (18):

$$\begin{aligned} a_2\left(e2\right) &= \frac{r_3}{1+e_2} \qquad \omega_2\left(t_3\right) = L_3\left(t_3\right) \\ \cos\left(\Delta L_{32}\left(e_2\right)\right) &= -\frac{1}{e_2}\left(\frac{r_3}{r_2}\left(1-e_2\right)-1\right) \end{aligned} \tag{17}$$

$$FTC_{32}\left(e_2, t_2\right) = 0 \rightarrow \left[e_2^{**}, t_2^{**}, t_3^{**}, a_2^{**}, w_2^{**}\right] \tag{18}$$

Fig. 11, Fig.12 and Fig.13 display the solution of the FTC for the eccentricity and post-encounter epoch, the dependency of time of flight and the associated semi-major axis on the shaping parameter and the porkchop plot obtained for the dates of post-encounter with Earth and arrival at Jupiter:

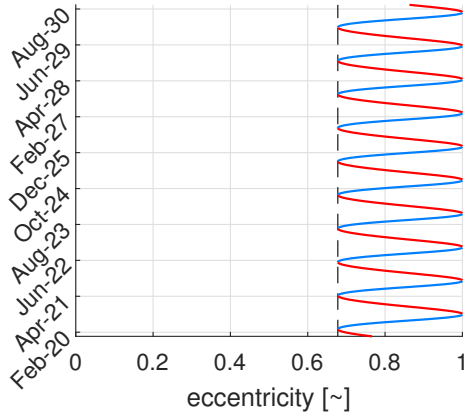

Figure 11: The correlation between the date of departure from Earth and the eccentricity for an orbit tangential at Jupiter, obtained from the feasible transfer condition. In light blue and red, respectively the short and long transfers

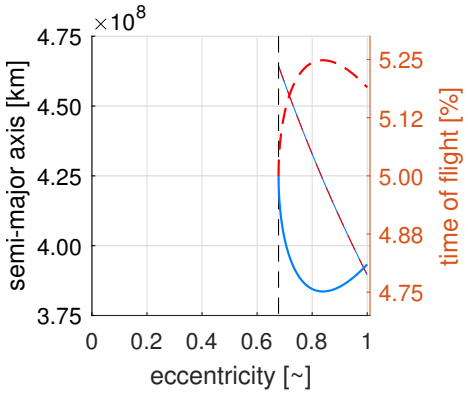

Figure 12: The evolution of the semi-major axis and the time of flight for a short (light blue) and long (red) transfer on the eccentricity.

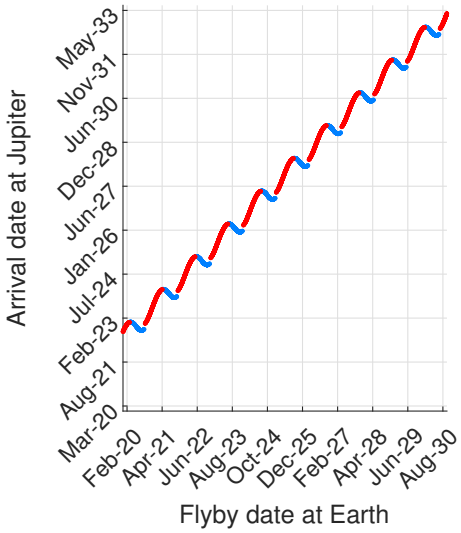

Figure 13: The FTC solutions expressed in departure/arrival dates for a tangential orbit on the arrival to Jupiter represented in a pork-chop plot manner. In light blue and red, respectively the short and long Earth-Jupiter transfers

The syzygy function shall identify where the solutions, described by (16) and (18) in the set of orbital elements and the departure and arrival time, merge at the flyby in term of encounter date and its effect on the variation of the orbital parameters.

The linearized orbit eq. variation

From the linearized orbit equation, see (8), one can see that at the flyby both conditions has to be verified, see (19):

$$\begin{aligned} \tfrac{p_1}{r_2} - f_1 \cos L_2 - g_1 \sin L_2 = 1 \\ \tfrac{p_2}{r_2} - f_2 \cos L_2 - g_2 \sin L_2 = 1 \end{aligned} \tag{19}$$

whose difference leads to the variational relation for the linearised orbit, see (20):

$$\frac{\Delta p}{r_2} - \Delta f \cos L_2 - \Delta g \sin L_2 = 0 \tag{20}$$

Considering that, the flyby occurs almost instantaneously, the variation of the equinoctial elements can be regarded as its derivative with the respect the time, and viceversa, which allows to rewrite (20) as function of the standard keplerian elements, see (21):

$$\begin{aligned} &\frac{\Delta a \left(1 - e^2\right)}{r_2} - \Delta e \left(\frac{2ae}{r_2} + \cos\left(L_2 - \omega\right) \right) - \\ &\Delta w \sin\left(L_2 - \omega\right) = 0 \end{aligned} \tag{21}$$

What (20) and (21) enunciate, is that after the flyby the trajectory must still be a conic which was exactly the desired policy to replace the initial line condition. Involving variations of orbital elements raised questions regarding the "sanity" of the formulation of the syzygy function which was tested with the Guass' planetary equations [5], see (22):

$$\begin{aligned} \tfrac{da}{dt} &= \tfrac{2a^2}{h} \left(e \sin f a_r + \tfrac{p}{r} a_\theta \right) \\ \tfrac{de}{dt} &= \tfrac{r}{h} \left\{ \tfrac{p}{r} \sin f a_r + \left[\left(1 + \tfrac{p}{r}\right) \cos f + e \right] a_\theta \right\} \\ \tfrac{d\omega}{dt} &= \tfrac{r}{he} \left[-\tfrac{p}{r} \cos f a_r + \left(1 + \tfrac{p}{r}\right) \cos f a_\theta \right) \end{aligned} \tag{22}$$

expressed as function of the disturbing acceleration, in radial and ortho-normal components, a_r and a_θ respictively. The zero function appears particularly nice since it is automatically satisfied for the Gauss solutions, meaning that when the syzygy function tends to zeros, it exists a real value for turning angle, δ, of the flyby such that the planetary encounter from a specific orbit, identified by $[a, e, \omega]$, induces the prescribed variations in orbital elements, and respectively in semi-major axis, Δa, eccentricity, Δe, and peri-apsis argument, $\Delta\omega$. In the end, it can be easily shown that the (21) is automatically satisfied in the one ellipse case.

The conic-syzygy solution can be written combining (21) with the FTC solutions, (16) and (18), into (23):

$$\begin{aligned} F = &\frac{\left(a_2^{**} - a_1^*\right)\left(1 - e_1^{*2}\right)}{r_2} + \\ &- \left(e_2^{**} - e_1^*\right) \left(\frac{2a_1^* e_1^*}{r_2} + \cos\left(\Delta L_{21}^*\right) \right) + \\ &- \left(\omega_2^{**} - \omega_1^*\right) \sin\left(\Delta L_{21}^*\right) \to 0 \end{aligned} \tag{23}$$

Nevertheless, there is a missing information on the maximum and minimum turning angles.

Gauss' planetary eq. applied to the flyby

Such problem can be faced studying rather than whether the value of turning angle associated to a given conic-syzygy, satisfies the limits, the variations of the orbital parameters with the respect of their maximum and minimum values obtained from the GPE (22).

To do that the disturbing acceleration, expressed in its radial and ortho-normal components, a_r and a_θ respectively, has to be defined for specific problem of the flyby. Again considering that the infinitesimal fraction of time during which the probe undergoes a flyby with the respect of his whole orbits, the derivative of the orbital element can be regarded as its variation as well as the acceleration can be interpreted as the variation of velocities [8]. In the hodograph representation [5], the heliocentric and infinity velocity at the encounter can be written as a function of the shape parameter, see (24) and Fig. 14:

$$\begin{aligned} \mathbf{v}\,(e) &= \tfrac{\mu}{h}\left(e\sin f\,\mathbf{i_r} + (1+e\cos f)\,\mathbf{i}_\theta\right) \\ \mathbf{v}_\infty\,(e) &= \tfrac{\mu}{h}\left(e\sin f\,\mathbf{i_r} + \left(1+e\cos f - \sqrt{\tfrac{p}{r}}\right)\mathbf{i}_\theta\right) \end{aligned} \tag{24}$$

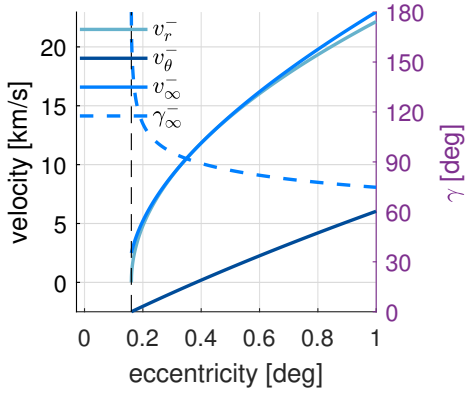

Figure 14: The entry angle and the relative velocity in its radial and ortho-normal components associated to the Venus-Earth leg

Which allows to write the pre- and post-encounter heliocentric velocity as a function of the components of the relative velocity, v_r^- and v_θ^-, the entry angle at infinite, γ^-, (displayed in Fig.14) and the turning angle at the flyby, δ, see (25):

$$\begin{aligned} \mathbf{v}^- &= \mathbf{v}_\infty\left(\sin\gamma^-\mathbf{i_r} + \cos\gamma^-\mathbf{i}_\theta\right) \\ \mathbf{v}^+ &= \mathbf{v}_\infty\left(\sin\left(\gamma^- \pm \delta\right)\mathbf{i_r} + \cos\gamma^- \pm \delta\mathbf{i}_\theta\right) \end{aligned} \tag{25}$$

where γ is the entry/exit angle described by the velocity at infinite with the respect to the planetary one, δ is the turning angle and the $\pm$ sign considers whether the flyby is retrograde or prograde.
Substituting the variations in radial and ortho-normal components, see (26):

$$\begin{aligned} \delta v_r &= v_\infty\left(\sin\gamma^+ - \sin\gamma^-\right) \\ \delta v_\theta &= v_\infty\left(\cos\gamma^+ - \cos\gamma^-\right) \end{aligned} \tag{26}$$

and differentiating with the respect of the exit angle, the value associated to the maximum/minimum variation of the three orbital elements can be identified by nullifying the derivative as function of the eccentricity, e, and the true anomaly, f only [7], see (27):

$$\begin{aligned} \gamma^+_{\Delta a_{MAX}} &= \arctan\left(\tfrac{e\sin f}{1+e\cos f}\right) \\ \gamma^+_{\Delta e_{MAX}} &= \arctan\left(\tfrac{(1+e\cos f)\sin f}{(2+e\cos f)\cos f+e}\right) \\ \gamma^+_{\Delta \omega_{MAX}} &= \arctan\left(-\tfrac{(1+e\cos f)\cos f}{(2+e\cos f)\sin f}\right) \end{aligned} \tag{27}$$

Whether those associated to the minimum variation can be easily obtained at π radiants difference, see (28):

$$\gamma^+_{\Delta a_{min}} = \gamma^+_{\Delta a_{MAX}} + \pi \tag{28}$$

and similarly for e and ω.

In our particular case, the problem simplify even further since the true anomaly is also function of the eccentricity, thus the exit angle for maximum/minimum variation can be parametrised as well and compared with the respect of the turning angle limits, see Fig.15.

Feasible values of the exit angle, γ^+, are those that satisfy the limits identified by the maximum and minimum turning angles, see (29):

$$\begin{aligned} \{\gamma_p^+| \quad & -\delta_{MAX} < \gamma^+ - \gamma^- \leq -\delta_{min}\} \\ \{\gamma_r^+| \quad & \delta_{min} \leq \gamma^+ - \gamma^- < \delta_{MAX}\} \end{aligned} \tag{29}$$

obtained for an encounter at the Sphere of Influence, associated to δ_{min}, and at the minimum periapsis, assigned to δ_{MAX}, see (30):

$$\begin{aligned} \delta_{min} &= \left(1 + \tfrac{v_\infty^2 a_{pl}}{\mu_{pl}^{4/5}\mu^{1/5}}\right)^{-1} \\ \delta_{MAX} &= \left(1 + \tfrac{v_\infty^2 r_{pl}}{\mu_{pl}}\right)^{-1} \end{aligned} \tag{30}$$

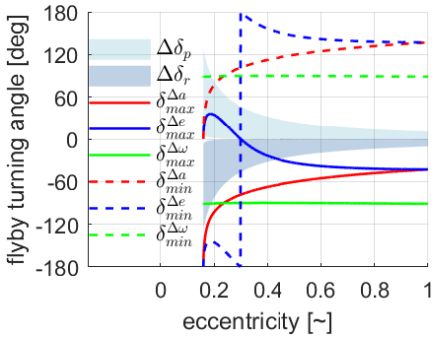

Figure 15: The turning angle, δ, for maximum/minimum variation obtained from the exit angle by diminishing its value of the entry angle. Red, blue and green lines, are associated to the variation in semi-major axis, eccentricity and argument of the periaspsis. Solid and dashed lines distinguish between the maximum and minimum variations respectively. Light and dark blue areas represent the limits for retrograde and prograde flyby

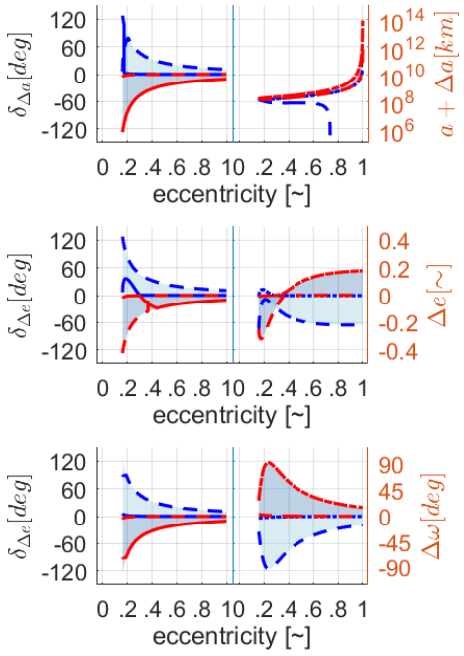

Figure 16: On the right, the turning angle for maximum/minimum variation, on the left, the associated range of maximum and minimum variations. From the top to the bottom, the values for semi-major axis, eccentricity and periaspsis argument. Blue and red lines distiguish between retro-/prograde flyby, while solid and dash lines between the max/min variations.

Defining the value of the turning angle within the limits, allows to determine feasible range for the assign orbital parameter, in particular see Fig.16

Given the formulation of the syzygy function, which involves an unconstrained turning angle,requires to evaluate their solutions with the respect to the four sets identified by (31) in term of matching flyby date and feasible boundary conditions for the orbital parameters variation:

$$\begin{gathered} t2^{**} == t2^{*} \\ \Delta a^{*}_{min} \leq a^{**}_{2} - a^{*}_{1} \leq \Delta a^{*}_{MAX} \\ \Delta e^{*}_{min} \leq e^{**}_{2} - e^{*}_{1} \leq \Delta e^{*}_{MAX} \\ \Delta w^{*}_{min} \leq w^{**}_{2} - w^{*}_{1} \leq \Delta w^{*}_{MAX} \end{gathered} \tag{31}$$

Solving the two orbits and one flyby problem in such manner is interesting since differently from the standard approach in which the patching of the hyperbolic trajectories has to be ensured, it offers the possibility to identify solutions with partial agreement with the constraints identified by (31), leaving the task to an optimizer to identify the overall refined trajectory, if exists.

5. Results

For the Earth-Venus-Jupiter trajectory, the solution of the conic-syzygy function can be compared with those identified by the in-range orbital variation approach. It must be stated that if the former approach offer a resolution defined for a unique turning angle, the latter identifies only upper and lower limits for the orbital element considered alone or in other terms that a set of variations $[\Delta a, \Delta e, \Delta\omega]$ within the limit might still produce an non-patched trajectories (not unique δ). By representing the solution for the conic-syzygy on top of the fully and partially satisfied limits 31, the porkchop plots assigned to first and second legs, Fig.18, and the shaping parameters map, Fig.17, display three different situations:

- solutions fully satisfying the boundary conditions, whose orbit sample is represented in Fig.19;
- solutions partially satisfying the boundary conditions, see Fig.20;
- solutions not satisfying the boundary conditions, see Fig.21.

.

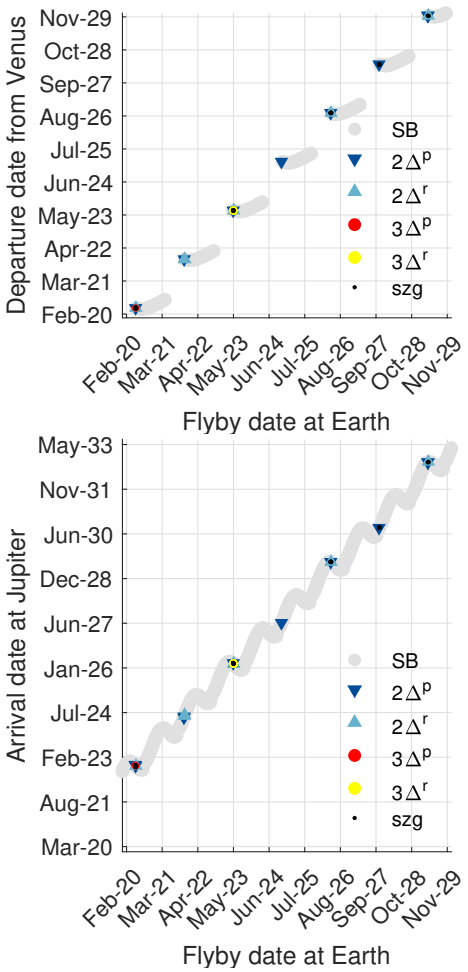

Figure 17: The pork-chop plots for the Venus-Earth and Earth-Jupiter legs. The dark and light blue circles identifies solutions with partial (two over three) agreements with the constraints, see (31), while the red and yellow ones the fully compliant ones, respectively for prograde and retrograde motion. The black dots represents the solutions of the conic-syzygy.

It is interesting to notice from Fig.19 and Fig.20 that, the solutions of the conic-syzygy captures both areas where the constraints are fully and only partially satisfied. It is highly probable that in the latter case, the optimiser might require a manoeuvre to obtain such an orbit, but a small delta-v is expected.

The fact that the fully compliant area in Fig.18 is not covered with black dots, assigned to the solutions of the syzygy function, can be associated to the fact that the syzygy resolves automatically the trajectory for a unique turning angle while the ranges don't. In the end, the out-layers must be analysed with particular attention but it is expected to identify an unfeasible solution.

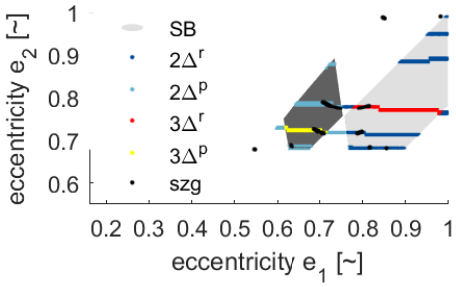

Figure 18: The shaping parameters correlation at the flyby. The dark and light gray areas represents the limits identified by the maximum and minimum variation of eccentricity and semi-major axis, respectively for prograde and retrogade motion. The dark and light blue circles identifies solutions with partial (two over three) agreements with the constraints, see (31), while the red and yellow ones the fully compliant ones, respectively for prograde and retrograde motion. The black dots represents the solutions of the conic-syzygy.

This can be done by evaluating the orbits associated to the solutions identified by the conic-syzygy function, here represented collected by year of departure for simplification, see Fig.21:

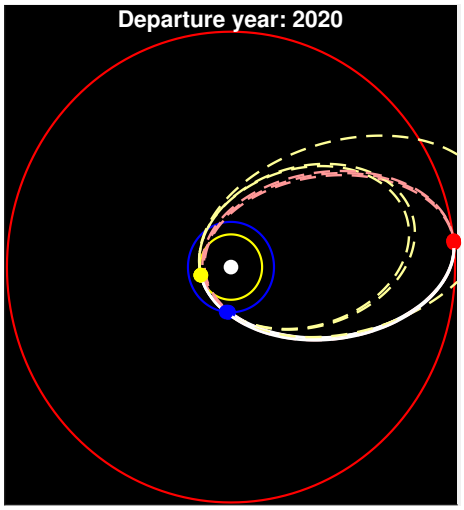

Figure 19: The trajectory obtained for a conic-syzygy solution fully compliant with the variational limits, hitting the the red/yellow area obtained for prograde and retrograde motion.

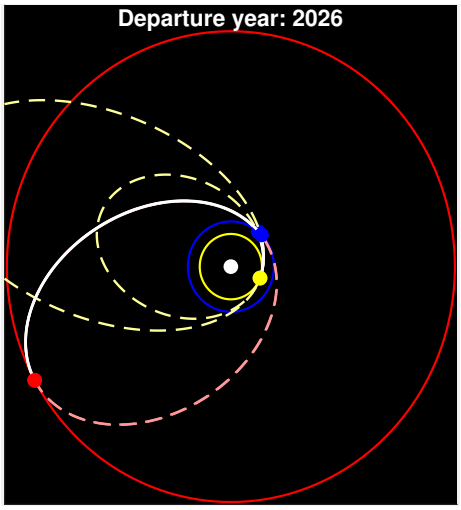

Figure 20: The orbit associated to a partial agreement of the constraints identified by the location of the syzygy solution over light/dark blue area assigned to prograde and retrograde motion.

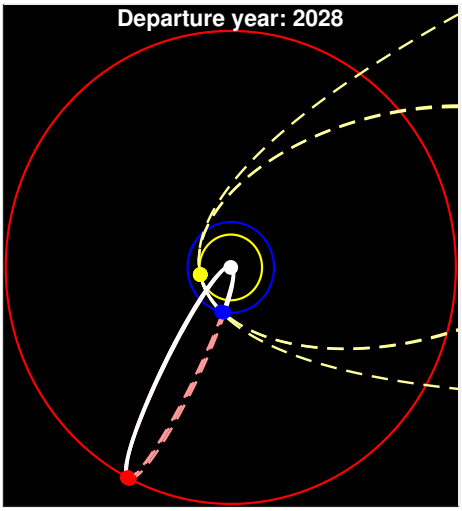

Figure 21: The trajectory obtained for an outlayer solution of the conic-syzygy method.

6. Conclusion

In conclusion, the objectve of this paper was to show the steps that brought to define the conic-syzygy function from its standard application. Although its results must still be proven to be optimal, theoretical evidence was provided. In the end, preliminary results show a good adherence between the solution of the linearised orbit eq. variation and the in-range approach, which makes the method promising, considering that no non-linear equation has been resolved. The outlayers solution represents a drawback of the method but the idea behind the paper was to provide preliminary solutions, which can still be discarded by the following stage of optimisation.

7. Future work

A way to handle the outlayers is currently under devolopment. Solutions for the syzygy function that doesn't tend to zero but that are within a certain small range, wants to be analyse in deep and their behaviour explained. Opitimality for the conic-syzygy function will be also checked. In the end, it is forseen to extend the work to the MGA case, considering a prescribed variation in eccentricity per flyby.

8. Acknowledgement

This project has received funding from the European Research Council (ERC) under the European Union's Horizon 2020 research and innovation programme (grant agreement No 679086 - COMPASS).

References

[1] Shane D Ross and Daniel J Scheeres. Multiple gravity assists, capture, and escape in the restricted three-body problem. *SIAM Journal on Applied Dynamical Systems*, 6(3):576–596, 2007.

[2] Stefano Campagnola and Ryan P Russell. Endgame problem part 2: multibody technique and the tisserand-poincare graph. *Journal of Guidance, Control, and Dynamics*, 33(2):476–486, 2010.

[3] Stefano Campagnola, Paul Skerritt, and Ryan P Russell. Flybys in the planar, circular, restricted, three-body problem. *Celestial Mechanics and Dynamical Astronomy*, 113(3):343–368, 2012.

[4] Elisa Maria Alessi and Joan Pau Sánchez. Semi-analytical approach for distant encounters in the spatial circular restricted three-body problem. *Journal of Guidance, Control, and Dynamics*, 39(2):351–359, 2015.

[5] Richard H Battin. *An introduction to the mathematics and methods of astrodynamics*. Aiaa, 1999.

[6] John E Prussing and Bruce A Conway. *Orbital mechanics*. Oxford University Press, USA, 1993.

[7] D Menzio and C Colombo. An analysis of the pork-chop plot for direct and multi-revolution flyby missions. In *4th IAA Conference on Dynamics and Control of Space Systems (DyCoSS 2018)*, pages 1–6, 2018.

[8] Camilla Colombo, Gianmarco Radice, and Massimiliano Vasile. *Optimal trajectory design for interception and deflection of Near Earth Objects*. PhD thesis, University of Glasgow, 2010.